; **AD-A268 776**

WL-TR-92-7035

Interferometer Stations at the Air Force Aeroballistic Research Facility

R. C. Anderson
J. E. Milton

University of Florida
P.O. Box 1918
Eglin AFB FL 32542

DTIC
ELECTE
AUG 3 0 1993
S B D

JULY 1993

FINAL REPORT FOR PERIOD AUGUST 1988 - DECEMBER 1990

93-20223

93 8 27 114

WRIGHT LABORATORY, ARMAMENT DIRECTORATE
Air Force Materiel Command ∎ United States Air Force ∎ Eglin Air Force Base

NOTICE

When Government drawings, specifications, or other data are used for any purpose other than in connection with a definitely Government-related procurement, the United States Government incurs no responsibility or any obligation whatsoever. The fact that the Government may have formulated or in any way supplied the said drawings, specifications, or other data, is not to be regarded by implication, or otherwise as in any manner construed, as licensing the holder, or any other person or corporation; or as conveying any rights or permission to manufacture, use, or sell any patented invention that may in any way be related thereto.

This technical report has been reviewed and is approved for publication.

FOR THE COMMANDER

Robert F Donohue

ROBERT F. DONOHUE, JR., Lt Col, USAF
Chief, Weapon FLight Mechanics Div

Even though this report may contain special release rights held by the controlling office, please do not request copies from the Wright Laboratory, Armament Directorate. If you qualify as a recipient, release approval will be obtained from the originating activity by DTIC. Address your request for additional copies to:

> Defense Technical Information Center
> Cameron Station
> Alexandria VA 22304-6145

If your address has changed, if you wish to be removed from our mailing list, or if your organization no longer employs the addressee, please notify WL/MNAA, Eglin AFB FL 32542-6810, to help us maintain a current mailing list.

Do not return copies of this report unless contractual obligations or notice on a specific document requires that it be returned.

REPORT DOCUMENTATION PAGE

Form Approved
OMB No 0704-0188

1. AGENCY USE ONLY (Leave blank)	2. REPORT DATE July 1993	3. REPORT TYPE AND DATES COVERED Final, August 1988 - December 1990

4. TITLE AND SUBTITLE Interferometer Stations at the Air Force Aeroballistic Research Facility	5. FUNDING NUMBERS PE: 62602F PR: 2567 TA: 03 WU: 23
6. AUTHOR(S) R. C. Anderson J. E. Milton	

7. PERFORMING ORGANIZATION NAME(S) AND ADDRESS(ES) University of Florida P.O. Box 1918 Eglin AFB FL 32542	8. PERFORMING ORGANIZATION REPORT NUMBER

9. SPONSORING/MONITORING AGENCY NAME(S) AND ADDRESS(ES) Wright Laboratory, Armament Directorate Weapon Flight Mechanics Division Aerodynamics Branch (WL/MNAA) Eglin AFB FL 32542-6810	10. SPONSORING/MONITORING AGENCY REPORT NUMBER WL-TR-92-7035

11. SUPPLEMENTARY NOTES

12a. DISTRIBUTION/AVAILABILITY STATEMENT Approved for public release; distribution is unlimited.	12b. DISTRIBUTION CODE A

13. ABSTRACT (Maximum 200 words)

Two interferometer stations were installed in the Eglin AFB ballistic range--a holographic and a common path interferometer. The latter was used in both dark central ground and field absorption modes. A theoretical development given for the common path instrument predicts an improved type of phase contrast interferometer with a half wave shifting filter instead of the quarter wave used in the past. Experimentally measured interferograms were found to be in good agreement with synthetic interferograms calculated with data from a Navier-Stokes Computational Fluid Dynamics (CFD) code.

14. SUBJECT TERMS Interferometer, Holography, Flow Visualization, Ballistics Test			15. NUMBER OF PAGES 41
			16. PRICE CODE

17. SECURITY CLASSIFICATION OF REPORT UNCLASSIFIED	18. SECURITY CLASSIFICATION OF THIS PAGE UNCLASSIFIED	19. SECURITY CLASSIFICATION OF ABSTRACT UNCLASSIFIED	20. LIMITATION OF ABSTRACT SAR

NSN 7540-01-280-5500

Standard Form 298 (Rev 2-89)
Prescribed by ANSI Std 239-18
298-102

PREFACE

This report documents the development of two interferometer
stations for use in the Aeroballistic Research Facility (ARF),
Eglin AFB, Florida. The stations were developed by the University
of Florida, Graduate Engineering Research Center, Eglin AFB,
Florida, under Contract F08635-88-C-0160 with WL/MN. Lt Mike
Stephens, WL/MNAA, managed the program for the Wright Laboratory,
Armament Directorate. This program was conducted during the period
from August 1988 to December 1990.

DTIC QUALITY INSPECTED 3

iii/iv (Blank)

TABLE OF CONTENTS

LIST OF FIGURES

LIST OF TABLES

SECTION I

INTRODUCTION

1. PURPOSE

The purpose of this effort was to produce interferometer stations in the ARF located at Eglin Air Force Base, Florida. The installations are needed to provide data for the experimental verification of Computational Fluid Dynamics (CFD) calculations and for high quality flow visualization.

2. BACKGROUND

Interferometry of fluid flows has, for a century (1891), been done primarily with Mach-Zehnder interferometers, which are well known for their sensitivity to environmental temperature changes and vibrations. In addition, the Mach-Zehnder requires very high quality optics, so instruments with sizable apertures are very expensive. These qualities eliminate this type of instrument for application in the ARF.

A new type of interferometer became available for flow measurements when Horman (Reference 1) suggested in 1965 that holography could be applied. Of the several types of holographic interferometers available, the one of interest here is the double-exposure hologram. This hologram is made in any of a number of standard setups where a single photographic plate is exposed twice. The first and second exposures are made of the object under two different conditions. When the hologram is reconstructed, two images are formed. The light from these images interfere to produce fringes showing the changes that have occurred in the time interval between exposures. In the case of the ARF, the first exposure is made of the undisturbed test area, and the second exposure is made as a projectile is passing. The fringes obtained represent changes that have occurred in the density field caused by the entry of the object.

The advantages of holographic interferometers compared to the Mach-Zehnders are that they are insensitive to temperature changes and vibrations because alignment is not critical and the very short exposures freeze any motion in time. Also, the optical components required are small and therefore relatively inexpensive. A description of the double-pulsed holography station installed in the ARF is given in Section II.

There are also a number of other interrelated inter- ferometers that predate holography and are very useful for quantitative measurements in fluid mechanics. Beginning with Prescott and Gayhart (Reference 2) and expanded upon by Erdmann (Reference 3), these have been discovered and rediscovered at

1

different times but inexplicably have never gained wide usage. There are four useful features: (1) they are insensitivite to vibrations and temperature changes, (2) interferograms are obtained directly without reconstruction, (3) many existing schlieren systems can be converted to interferometers, and (4) these interferometers are inexpensive when compared to the Mach-Zehnder.

Two types were used successfully in the ARF, one based upon a technique known as dark central ground and the other based upon field absorption. These methods, along with another that has not been tried experimentally, are discussed in detail in Section III.

SECTION II

HOLOGRAPHIC INTERFEROMETER

1. INSTALLED INTERFEROMETER

Because holographic interferometry is, in general, a well-documented science, the basics will not be repeated here. There are many good reviews available, e.g., Vest (Reference 4) and Merzkirch (Reference 5). The major difference between the interferometer discussed here and many of those reported in other places is the scale.

Figure 1 shows the ARF optical layout. Table 1 identifies the components indicated in the figure. Light from a ruby laser enters through an opening in the concrete wall separating the tunnel area from the hall where much of the instrumentation is located. The laser is a double-pulse ruby operated in the TEMoo mode with approximately 30 millijoules of energy that can be divided equally between the two pulses. The beam is split into object and reference beams by an uncoated glass beam splitter, which splits off about 4 percent of the original beam to form the reference beam. The second surface of the beam splitter is tipped 30 arc minutes with respect to the front surface in order to produce a divergence of the reflections from the two surfaces. This makes it possible to block the second reflection at the mirror M3.

The reference beam goes from the beam splitter to M3, is folded to cross the tunnel, and is again folded at M4. The beam is then expanded by the lens L2 and folded by M5 to illuminate the liquid gate plate holder. A commercially available liquid gate, filled with xylene, is used to match the index of refraction of the film emulsion. The xylene reduces the effects of phase variations caused by uneven film thickness and also the reflectance of the back surface of the film plate. The film used was AGFA 10E75 nonAH coated glass plates.

The object beam is passed through the beam splitter and folded by M1. It is necessary to use a dielectric mirror at M1 to withstand the irradiance without damage. After folding, lens L1 expands the beam that is again folded by M2 to illuminate the scattering screen attached to the back wall. It is necessary to make L1 a negative lens to prevent air breakdown at the focus. Beaded auto—reflecting tape on a sturdy panel is used for a scattering screen. The return from the screen is so highly directional that the angle between M2 and the liquid gate, as seen from the screen, has to be as small as possible. Also, the normal to the holographic plate bisets the angle formed by M5, LG, and the scattering screen center.

3
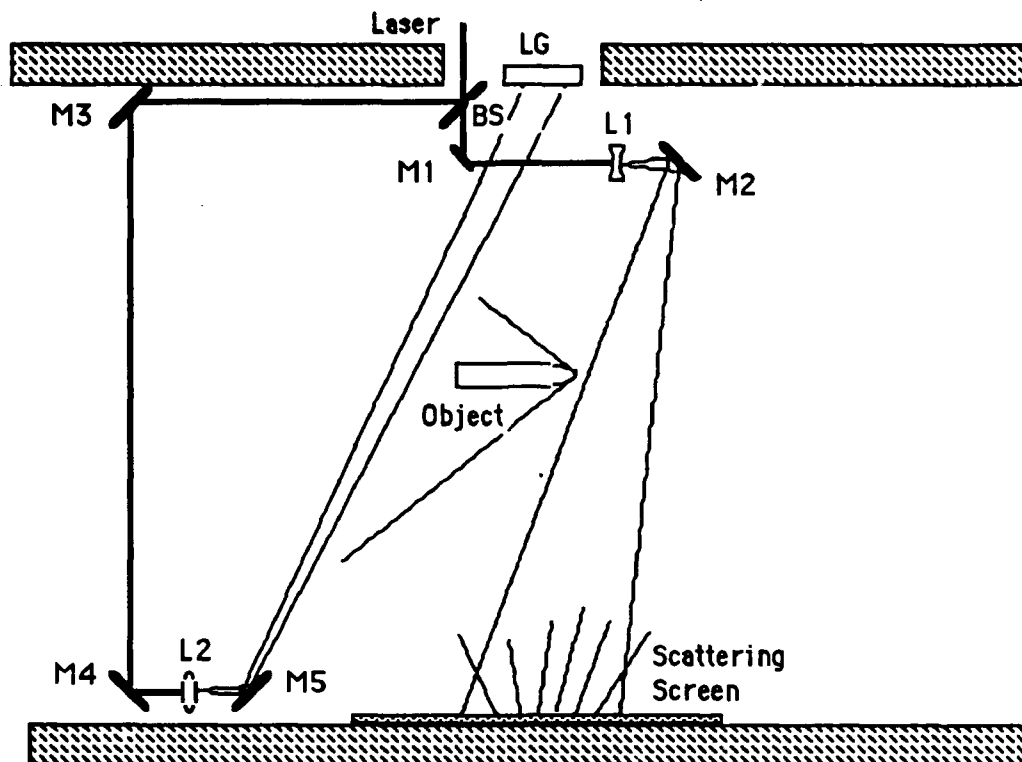
Figure 1.   Optical Layout for the Holographic
Interferometer Used in the ARF

Table 1. OPTICAL COMPONENTS FOR THE HOLOGRAPHIC STATION

Symbol	Element
Laser	Double-pulse ruby laser
BS	Uncoated glass beam splitter
L1	Negative expanding lens
L2	Positive expanding lens
M1	Dielectric flat mirror
M2	Aluminized flat mirror
M3	Aluminized flat mirror
M4	Aluminized flat mirror
M5	Aluminized flat mirror
LG	Liquid gate plate holder

Figure 1 shows the standard method for recording a hologram
of a diffusely reflecting object--for example, the scattering

4

screen. The actual object of interest, the flow about the projectile, is backlighted by the screen. Each exposure records a hologram of the screen as viewed through the air between the screen and the liquid gate. On the first exposure, the projectile and the disturbed air around it have not entered the field so that the first hologram is of the screen as viewed through the air in the tunnel. This air is neither uniform nor stationary. As judged by observing the real-time interferograms from the dark central ground interferometer described later, the average phase shifts seem to be a random one or two waves. The second exposure, on the same plate, records the screen as viewed through the tunnel air and the flow field around the projectile.

When the double-exposure hologram is reconstructed, two superimposed images are formed. The small differences in phase of the light show up as interference fringes. The composite is the interferogram. Changes between exposures can be caused by relative motion between the components or by changes in the air path. Of most concern are the changes in the air path and vibration of the scattering screen caused by acoustic waves propagating within the concrete walls.

2. EXAMPLE EXPERIMENTAL RESULTS

Typical examples of interferograms obtained from the reconstructed holograms are shown in the following figures. Figure 2 shows the interferogram of the flow field about a sphere traveling at a Mach number slightly above one. This interferogram illustrates the power of the system by showing the extreme detail that was obtained within the bow wave of the flow.

Figure 3 is the interferogram of the flow about a cone-cylinder-flare traveling at a Mach number of approximately 3 with zero angle of attack. The cone half angle is 22.5 degrees; the cylindrical section has a diameter of 1.91 centimeters (cm) and a length of 1.91 cm. The flare angle is 10 degrees and the axial length is 5.32 cm.

Figure 4 is the interferogram of the flow about a cone-cylinder-ogive traveling at a Mach number of 3.17. The cone half angle is 10 degrees; the cylindrical section has a diameter of 1.91 cm and a length of 3.68 cm. The ogive base length is 1.71 cm. The model is flying at a positive angle of attack.

Figures 5 and 6 are the interferograms of a cone with a half angle of 10 degrees and a length of 5.4 cm with a base diameter of 1.91 cm. The cone in Figure 5 is moving at Mach 3.03; in Figure 6, the Mach number is 3.87. In Figure 6, the projectile has a negative angle of attack of approximately 5 degrees, while in Figure 5 the angle of attack is positive with a value of approximately 2 degrees. Figures 7 and 8 are synthetic

interferograms obtained by Butler et. al. (Reference 6) for the cone seen in Figures 5 and 6. Figure 7 corresponds to zero angle of attack and a Mach number of 3.03. Comparing the synthetic interferogram to the experimental one shown in Figure 5, it is seen that the agreement is very good. The qualitative aspects of the flow have been successfully simulated by the synthetic interferogram.

A zero angle of attack and a Mach number of 3.87 is assumed for Figure 8. Comparison with Figure 6 shows that the correlation, while still surprisingly good, is not as good as in the previous case. This can probably be attributed to the nonzero angle of attack of the cone in the experimental case shown in Figure 6.
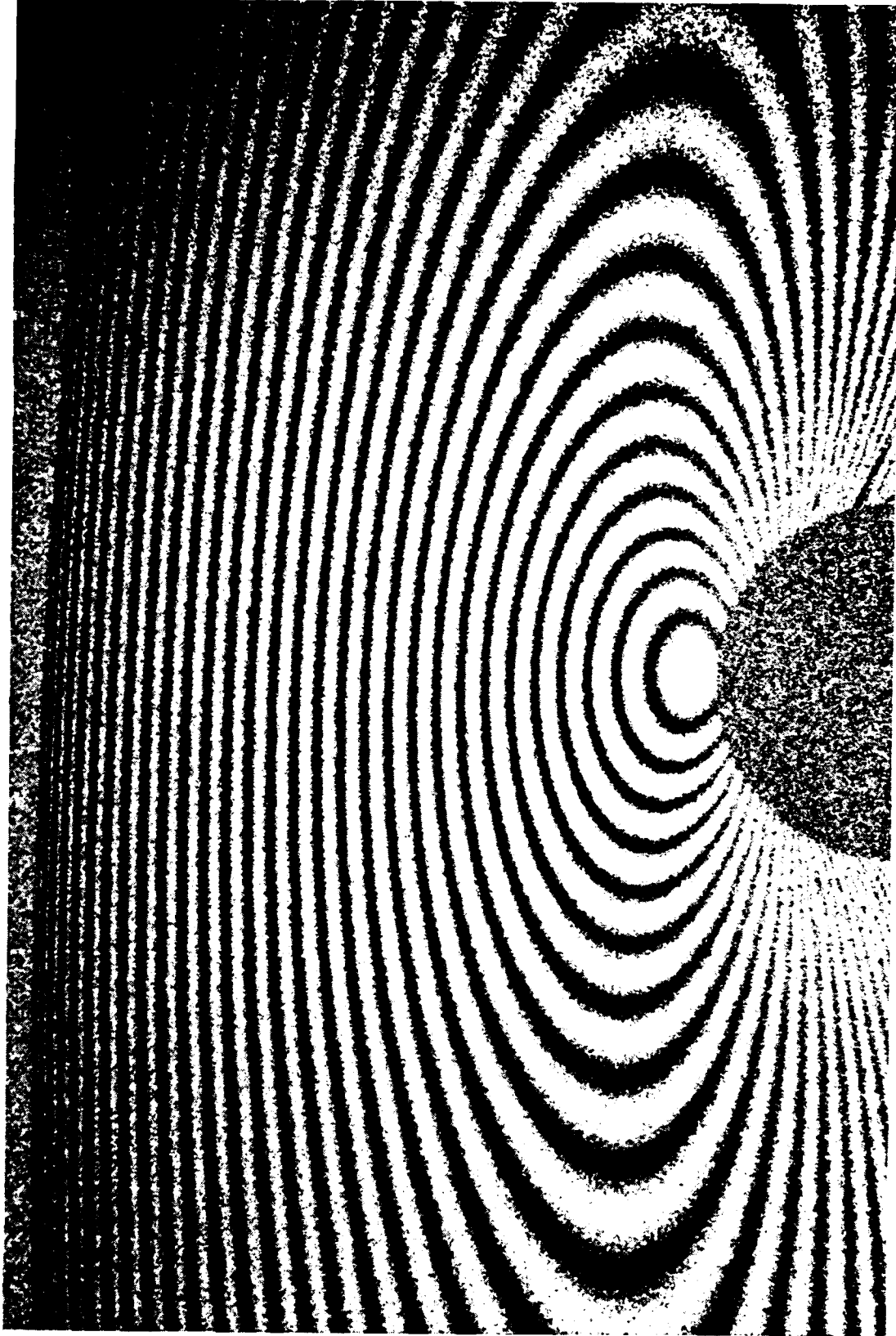
Figure 2. Interferogram of Flow About a Sphere

7

Figure 3. Interferogram of the Flow About the Cone Cylinder Flare Model
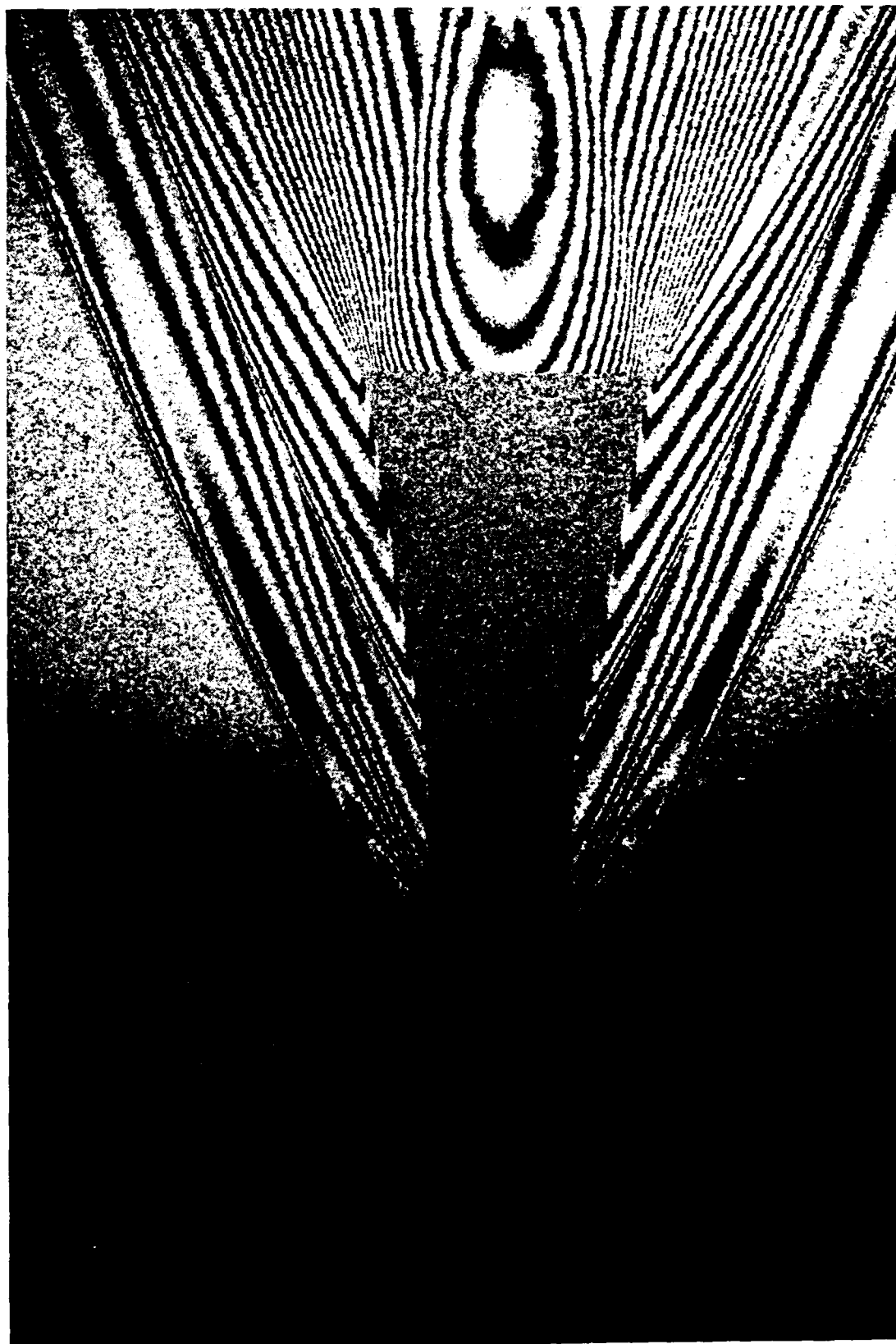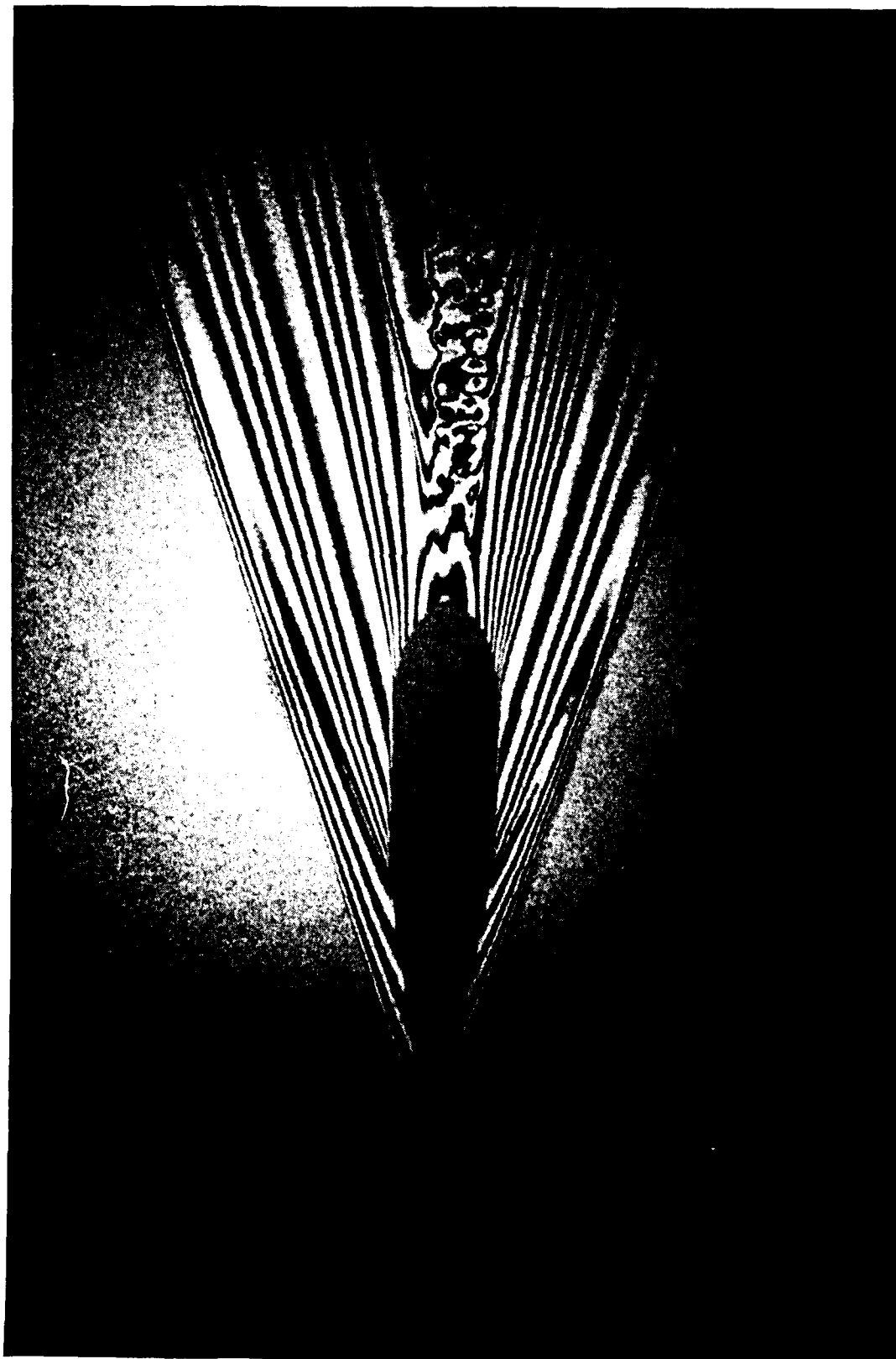
8

Figure 4. Interferogram of the Flow About the Cone Cylinder Ogive Model
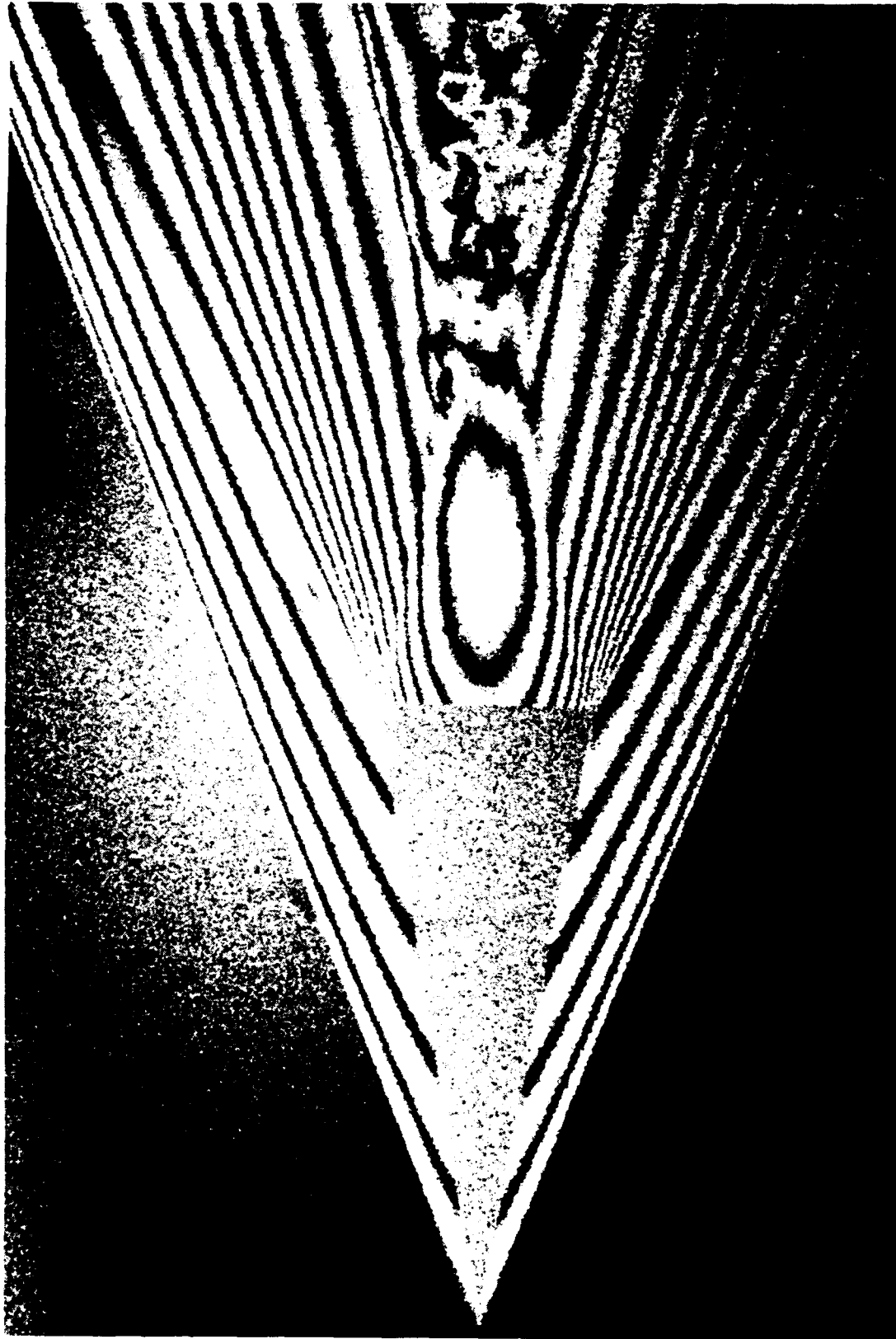
9

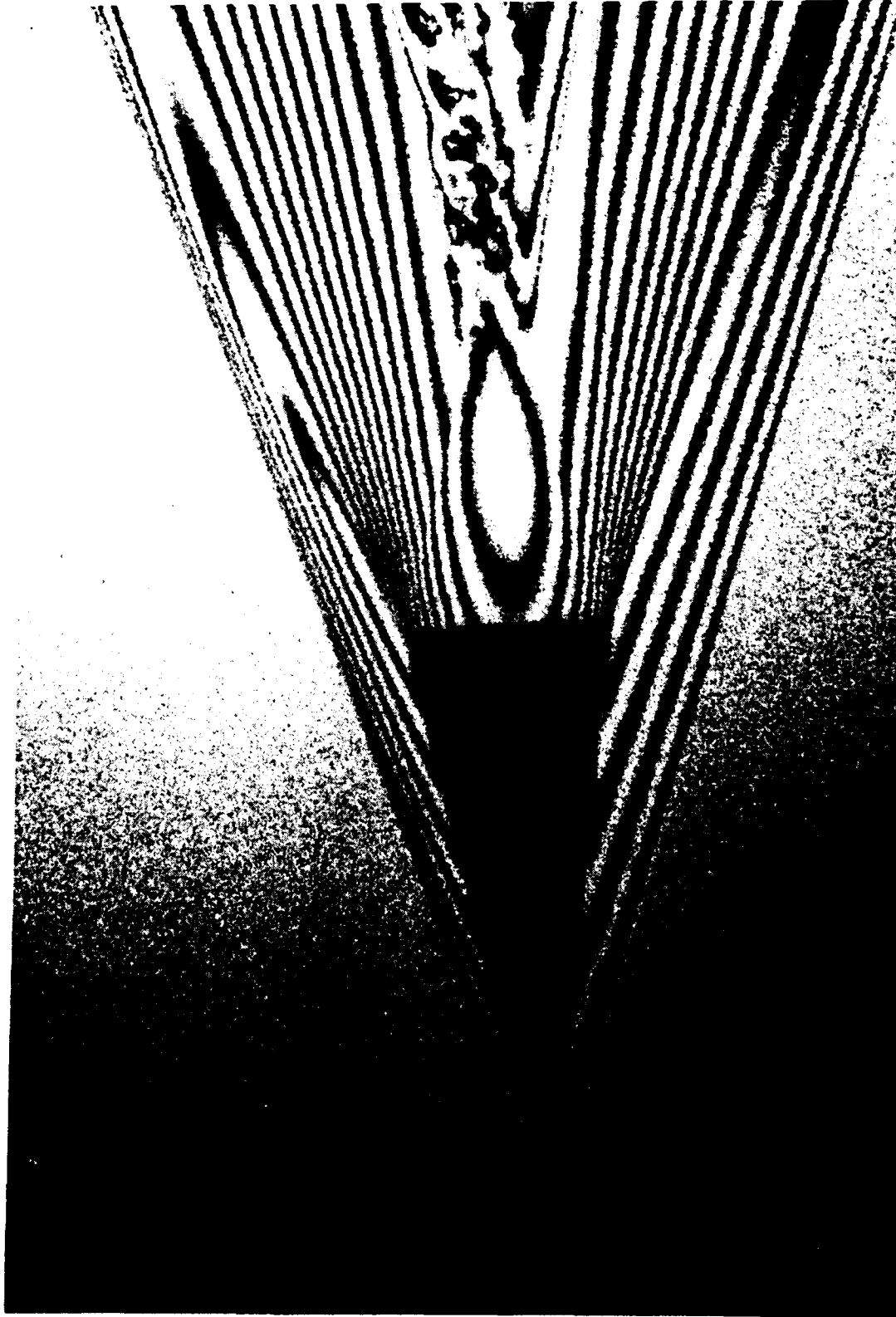Figure 5. Interferogram of the Flow About a Cone at Mach 3.03

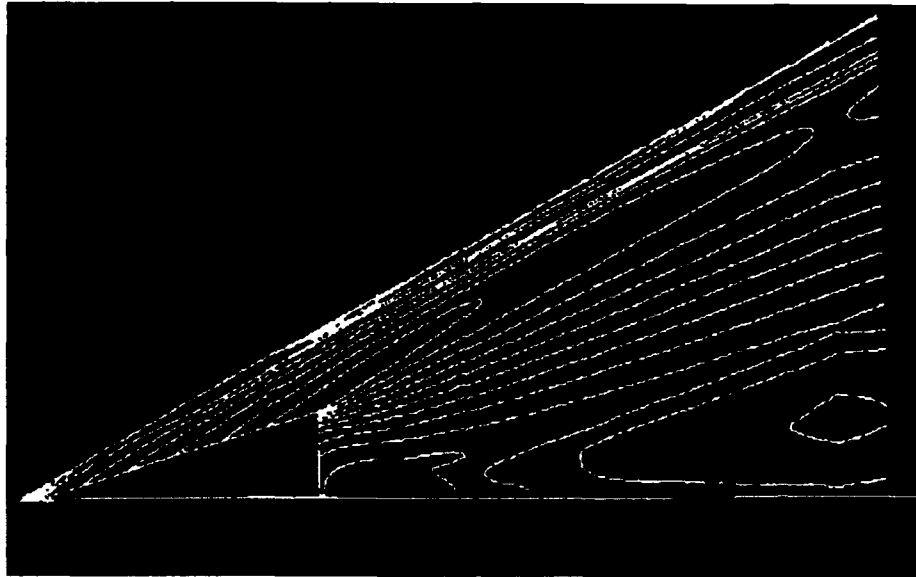Figure 6. Interferogram of the Flow About a Cone at Mach 3.87

11

Figure 7. Interferogram for the Flow About a Cone at Mach 3.03
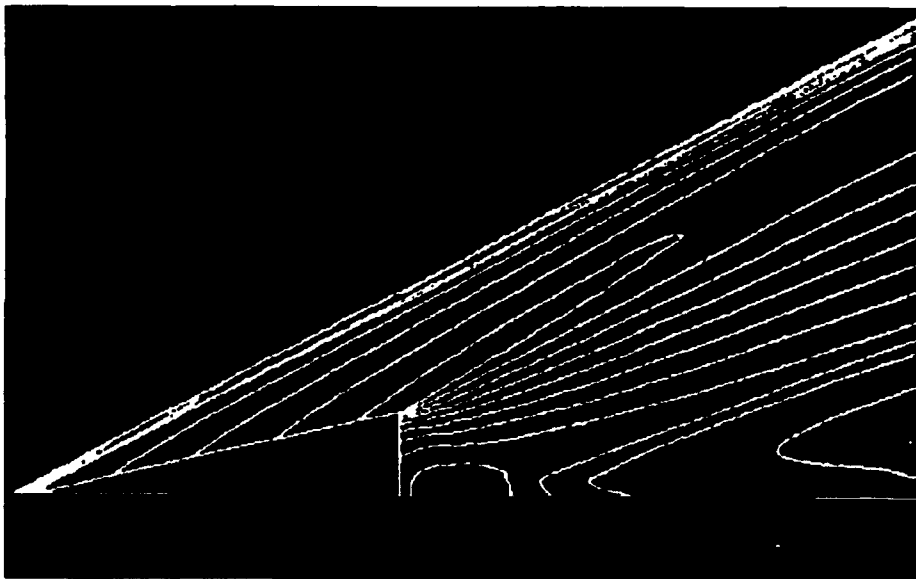
Figure 8. Synthetic Interferogram for the Flow About a
Cone at Mach 3.87

SECTION III

COMMON-PATH INTERFEROMETERS

1. GENERAL DESCRIPTION

A common-path interferometer is defined as an interferometer whose object and reference beams both follow very closely the same optical path. The major advantage is that when there are external influences--e.g., thermal changes or vibration--both beams tend to be affected in the same way and the output is unaffected. The common-path interferometers discussed in this section are the dark central ground, field absorption, and phase contrast types. They are all closely related optically to the schlieren system and the phase contrast microscope.

A basic schlieren optical layout, shown in Figure 9, will be used as a starting point for the description of each of the interferometers. However, the analysis will take a different viewpoint than the conventional one for interferometers in that these systems will be viewed as optical processors (Reference 7) with spatial filters modifying the light waves. The net result is that interferograms appear in the image plane.

The major changes required to produce an interferometer from a classical schlieren system are the replacement of the knife edge with a different element, to be described below, and the use of a laser source. The laser used for this work was a nonholographic quality pulsed ruby. It could also have been any continuous laser with enough power to make the required exposures.

Figure 9.   Basic Optical Layout for Three Common Path
            Interferometers

The first interferometer of this family, was reported by Prescott and Gaylord, loc. cit. Their source was a narrow slit illuminated by a mercury lamp. The spatial filter was a fine

13

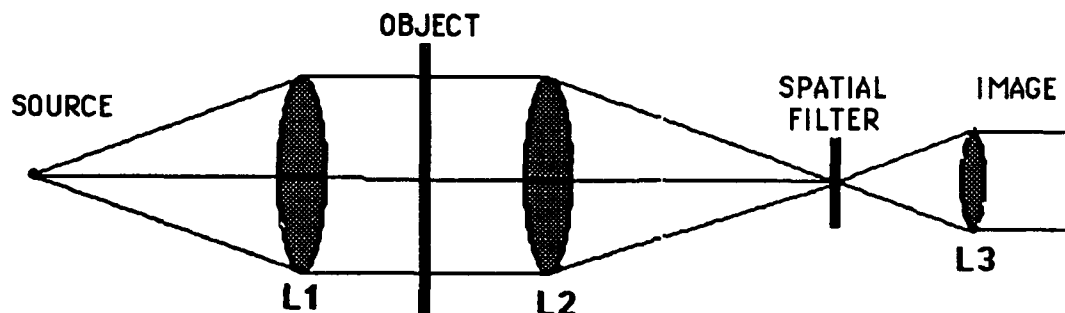wire placed at the focal point of L2, which blocked the image of the source. When the width of the slit was sufficiently narrow, fringes would appear in the flow field. These fringes were shown experimentally to correspond to fringes of constant column densities along the line of sight. It was also observed that the interferometer did not perform well when the density gradients were aligned with the direction of the wire. The technique turned out to be of limited use at that time because the weak light sources available caused photographic exposure times to be very long. While considered to be the first attempt to use the dark central ground method from microscopy, it was not recognized as such at the time.

The work of Prescott and Gaylord was explained theoretically and expanded by Erdmann loc. cit. Erdmann applied the methods Zernike (Reference 8) developed for phase contrast microscopy to the modification of schlieren systems into interferometers for flow studies. His work included phase contrast, dark central ground, and a new approach called field absorption. These techniques will be explained below. Erdmann's experimental work was still plagued by the necessity to use a slit source in order to have enough power to photograph the flows. As a result, he was unable to fully exploit the methods.

Since the early work on the subject, only a few isolated studies were done--e.g., Bouyer and Chartier (Reference 9) Philbert (Reference 10) and Veret (Reference 11) used phase contrast with objects having only small phase changes.

Optically the problems of flow visualization, testing of optical elements, and microscopy with transparent phase objects are all very similar. In each, phase distortions must be made visible. An interferometer, called the point-diffraction interferometer, used for testing the figure of telescope mirrors by Smartt and Strong (Reference 12) and by Smartt and Steel (Reference 13) was developed and used earlier for fluid flow by Erdmann with the name of field absorption, loc. cit. Anderson and Taylor (Reference 14) reported the use of phase contrast to produce interferograms of flow fields when the phase shifts were large. The dark central ground method was also applied to flow visualization problems by Anderson and Lewis (Reference 15) and found to be superior to the phase contrast method for multiple wavelength shifts in phase. They found that dark central ground gave bright fringes with good visibility. With about 15 milliwatts of laser power, 32 frames-per-second motion pictures were taken of a transient phenomenon, which, of course, produced a different interferogram in each frame.

Finally, Anderson and Milton (Reference 16) have shown experimentally that typical large aperture schlieren systems can easily be made into interferometers. They have tested two types:

14

the single pass 'Z' and the double pass, single mirror
configuration.

2.THEORY

In order to see how these systems operate, it is necessary
to abandon the refraction of optical rays approximation usually
used to explain schlieren systems and replace it with a wave
optics analysis. Figure 9 is a schematic drawing for one
possible optical layout. The source is assumed to be a laser
beam diverging from the front focal point of lens L1 so that
there is plane wave illumination in the test section. As the
light passes through the object, it can be altered in both
amplitude and phase at each point. Theoretically, these points
are treated as new point sources, each with its own amplitude and
phase that produce new outwardly propagating spherical waves-
-Huygens' wavelets. The complex amplitude of the light at any
point downstream is therefore just the sum of all the wavelet
amplitudes from all the points. If the wavelet summing is done
at infinity (far field), the result will be the amplitude of the
Fraunhofer diffraction pattern of the object.

It is this pattern that is altered by the spatial filter.
Lens L2 simply brings the pattern from infinity back to the focal
plane where it is accessible. The usual schlieren knife edge is
a spatial filter that allows one half of this diffraction pattern
to pass. This type of spatial filter does not result in an
interferometer. Other filter configurations, which do cause
schlieren systems to become interferometers, are described below.
If L3 is temporarily removed and the viewing screen is far enough
away from the spatial filter, a modified image of the object is to
be formed. If the spatial filter is a knife edge, a schlieren
image appears. This image is the Fraunhofer diffraction pattern
of the light from the plane just after the spatial filter. It is
the sum of the Huygens wavelets originating in the filter plane.
Lens L3 brings the final image to a desirable position and
establishes its size. The nature of the image depends upon how
the diffraction pattern of the object is altered as it passes
through the filter.

In mathematical terms, the complex amplitude of the
diffraction pattern in the back focal plane of L2 is given as
follows (Reference 7):

$$U(x_f,y_f) = \frac{C}{j\lambda f}\int\int_{-\infty}^{\infty} U(x_0,y_0)\exp[\frac{2\pi j}{\lambda f}(x_f x_0 + y_f y_0)]\,dx_0 dy_0 \qquad (1)$$

where $U(x_0,y_0)$ is the complex amplitude of the light after
passing through the object, C is a complex constant, f is the
focal length of L2, subscript f refers to the back focal plane,
x_0 and y_0 are the coordinates normal to the axis, and λ is the
wavelength of the light. Fortuitously, it turns out that the

15

integral is just the Fourier transform of the object multiplied by a complex constant. Ignore the constants in front of the integral and use the following shorthand notation to rewrite Equation 1:

$$U(x_f, y_f) = F\{U(x_0, y_0)\} \qquad (2)$$

where **F** indicates a Fourier transform. Equation 2 gives the amplitude of the light just before it passes through the spatial filter. The layout and nomenclature of the filters is shown in Figure 10.
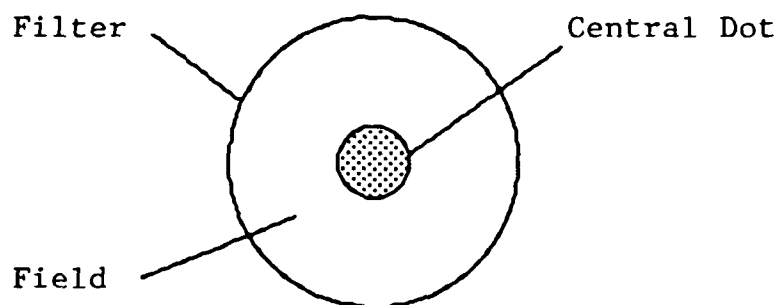
Figure 10. Example Spatial Filter

Three types of filters are considered:

a.   The dark central ground is so named because all the light falling on the central dot is blocked. The filter, $h(x_f, y_f)$, can be represented by

$$h(x_f, y_f) = 1 - circ(r/a) \qquad (3)$$

where r is the radial distance from the optical axis, a is the radius of the central dot, and

$$circ(r/a) = 1 \quad r \le a$$
$$= 0 \quad r > a.$$

b.   With field absorption all the light in the central dot is passed while the rest of the field is attenuated. The filter for this case is

$$h(x_f, y_f) = b + (1-b) circ(r/a) \qquad (4)$$

where b is the amplitude transmittance of the field.

c.   The third filter corresponds to the one used in phase contrast microscopy:

16

$$h(x_f, y_f) = 1 + [t \exp(j\pi/2) - 1] \, circ(r/a) \qquad (5)$$

where t is the amplitude transmittance of the central dot. In this case, the central dot attenuates the light and causes a quarter wave phase shift. The transmittance can be varied from one to zero to enhance contrast; however, when it equals zero, the phase contrast filter reduces to the dark central ground filter.

Light from Equation 2 passes through the filter and becomes

$$U'(x_f, y_f) = h(x_f, y_f) \, U(x_f, y_f). \qquad (6)$$

This light undergoes Fraunhofer diffraction to form the final image. Therefore, the complex amplitude in the image plane can be written as

$$U(x_i, y_i) = F\{h(x_f, y_f) F\{U(x_0, y_0)\}\}. \qquad (7)$$

If the filter for dark central ground is used in Equation 7 with the identity

$$F\{F\{U(x_0, y_0)\}\} = U(-x_0, -y_0), \qquad (8)$$

and with the convolution theorem, the amplitude of the image becomes

$$U(x_i, y_i) = U(-x_0, -y_0) - U(-x_0, -y_0) * F\{circ(r/a)\}. \qquad (9)$$

Negative signs on the coordinates indicate an inverted image. The asterisk denotes a convolution integral. The observed intensity distribution is equal to the magnitude of $U(x_i, y_i)$ squared or

$$I = |U_0|^2 + |U_0 * F\{circ(r/a)\}|^2$$
$$- U_0 [U_0 * F\{circ(r/a)\}]^* - U_0^* [U_0 * F\{circ(r/a)\}]. \qquad (10)$$

In Equation 10, the asterisks on the functions--e.g., U^*-- indicate complex conjugates. This equation has the appearance of a two-beam interference equation with $U_0^* F\{circ(r/a)\}$ replacing the reference beam. However, no such beam is actually identifiable within the system. What is actually happening is selected wavelets are being removed by the filter. If the proper set of wavelets are allowed to pass, they will interfere and form the desired interferogram.

3. CALCULATIONS

A one-dimensional thin prism is used as an object for all three filters. A unit amplitude plane wave twice the size of the prism is used for illumination. The prism has a linear Phase 1

17

shift from zero to five cycles and a transmittance of one.   A
plot of phase versus location in the field is shown in Figure 11.
The magnitude of the complex amplitude of the prism's diffraction
pattern is shown in Figure 12.   This diffraction pattern is used
to illuminate each of the three filters.   For comparison, the
diffraction pattern with the object removed from the field is
shown in Figure 13.   The effect of the object on the diffraction
pattern is to shift power away from the central peak. The
diffraction pattern of the light shown in Figure 12 is the object
inverted.

a. Dark Central Ground

    The dark central ground filter, given by Equation 3, is
applied first.   For a dark central ground interferometer, the
central dot is made just large enough to block the central peak
in Figure 13.   A plot is shown in Figure 14. Figure 15 is the
same as Figure 14 except the object has been put into the field.
The intensity of the diffraction pattern of the light that passes
through the filter forms the modified image, which is called an
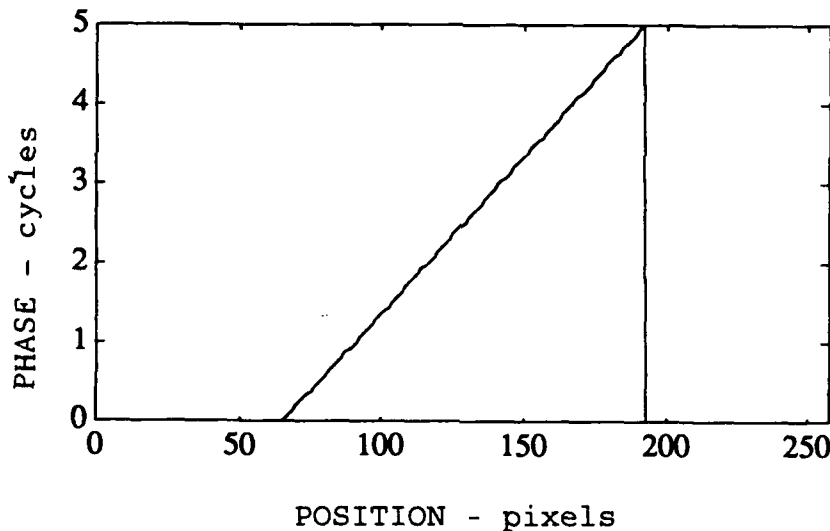interferogram. (See Figure 16).
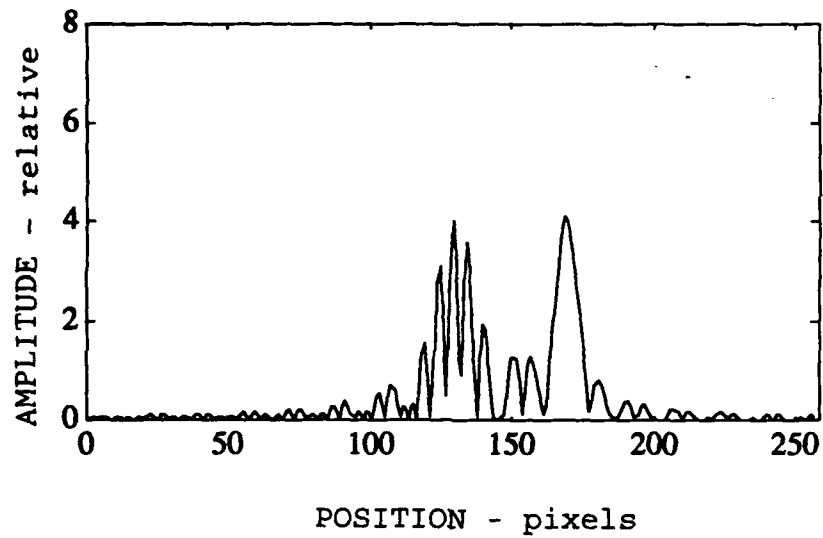
Figure 11. Example Phase Object

18

Figure 12. Diffraction with the Phase Object in the Field
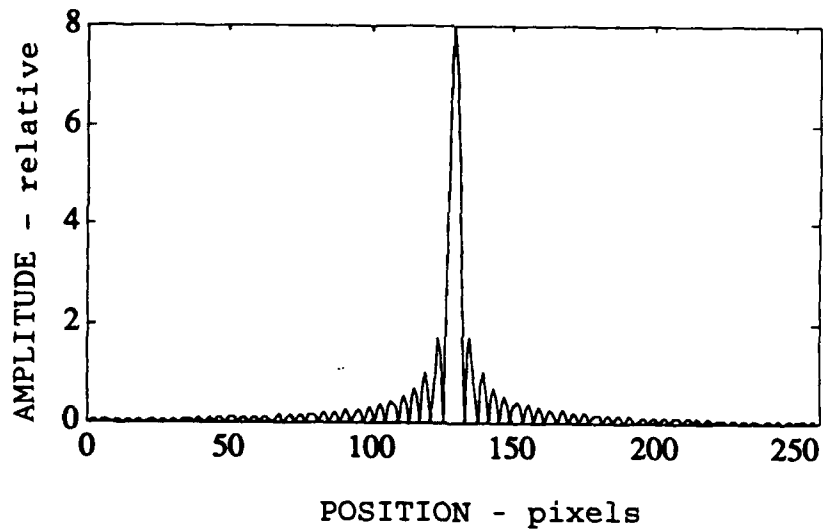
Figure 13. Diffraction Pattern with the Object Removed
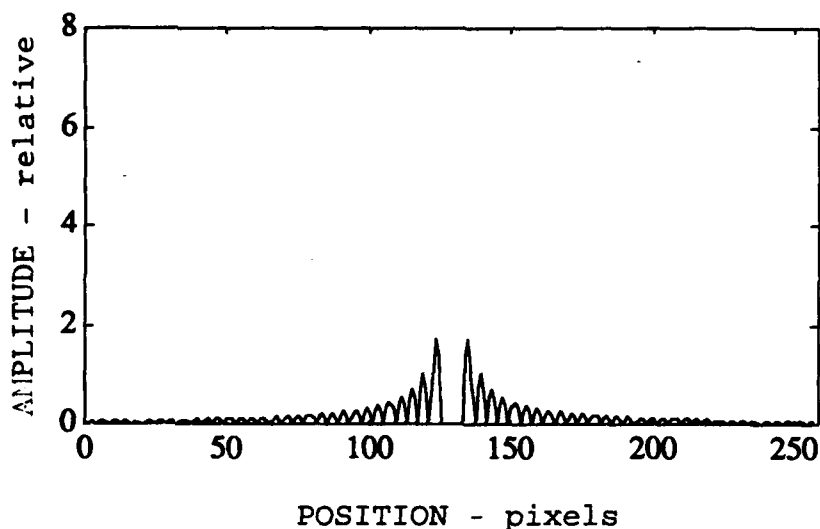
Figure 14. Filtered Pattern with an Undisturbed Field
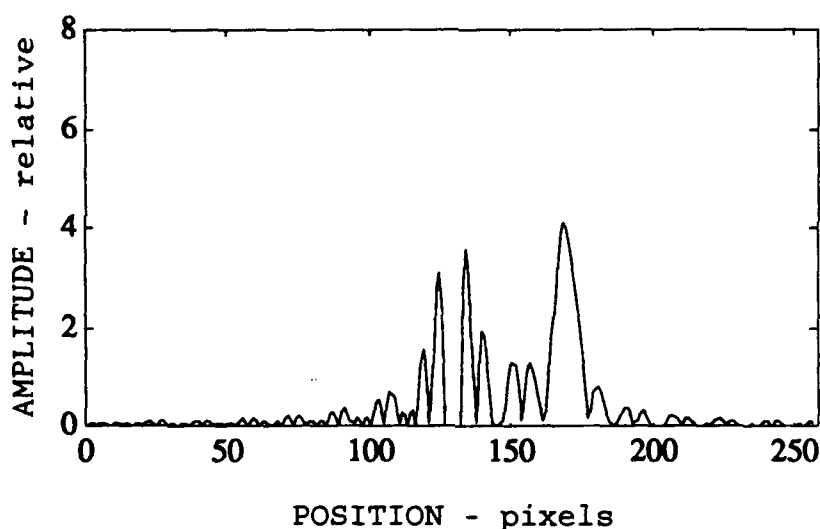
Figure 15. Filtered Pattern with the Object in the Field

The five-fringe image is the interferogram corresponding to the five cycles of phase shift caused by the object. The constant unit amplitude image, overlaid on the interferogram, is what would be seen if the filter was removed. Without a filter, the intensity is constant because the object is transparent and only shifts the phase of the light. An important point to note, in Figure 16, is that the number of bright fringes is proportional to the number of cycles of phase shift in the object. The phase shift is in turn proportional to the column density in aerodynamics. This relationship means the dark central ground interferometer produces interferograms with fringes entirely equivalent to those given by a Mach-Zehnder

20

interferometer, adjusted for infinite fringe, or to a single view reconstructed from a holographic interferometer.
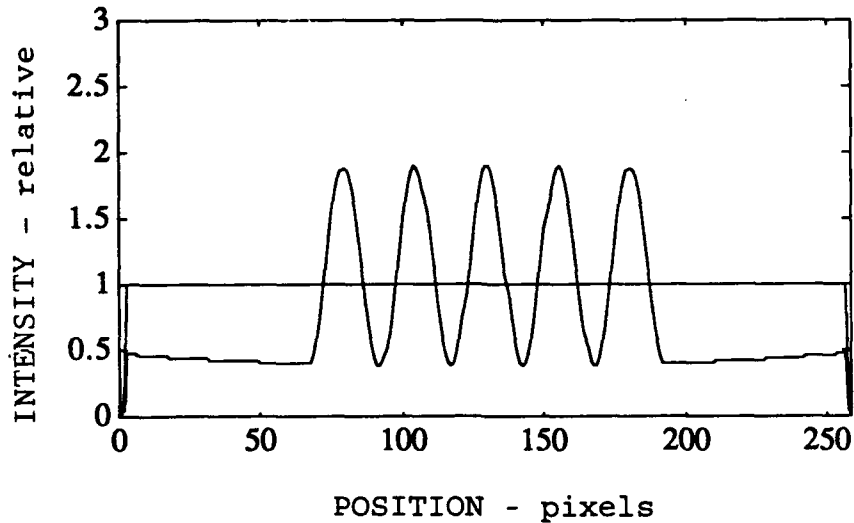
Figure 16. Image Intensity, Dark Central Ground

b.   Field Absorption

The same example is now repeated for a field absorption filter. This time the central dot is a clear aperture, and the field has an intensity transmittance of 0.0625. This value seems to give near-maximum fringe visibility. Figure 17 is the filtered spectrum corresponding to the one in Figure 15 for dark central ground. The resulting image is shown in Figure 18 to the same scale as Figure 16. Comparison of the results for field absorption and dark central ground reveals that there are five dark fringes in the field absorption image whereas there are five bright fringes with dark central ground. The two patterns are complimentary. Fringe visibility is improved for field absorption, but the intensity is down by nearly an order of magnitude. This situation could be a drawback in high speed work.

21
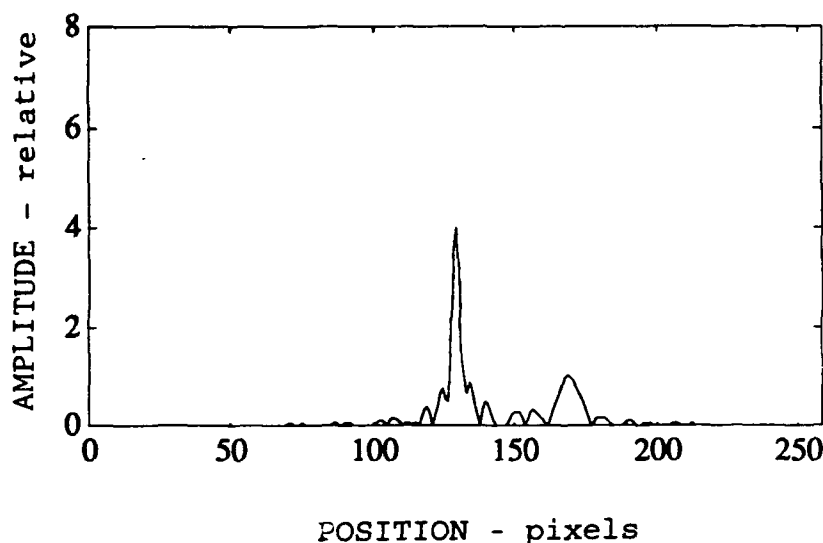
Figure 17. Filtered Spectrum with Field Absorption
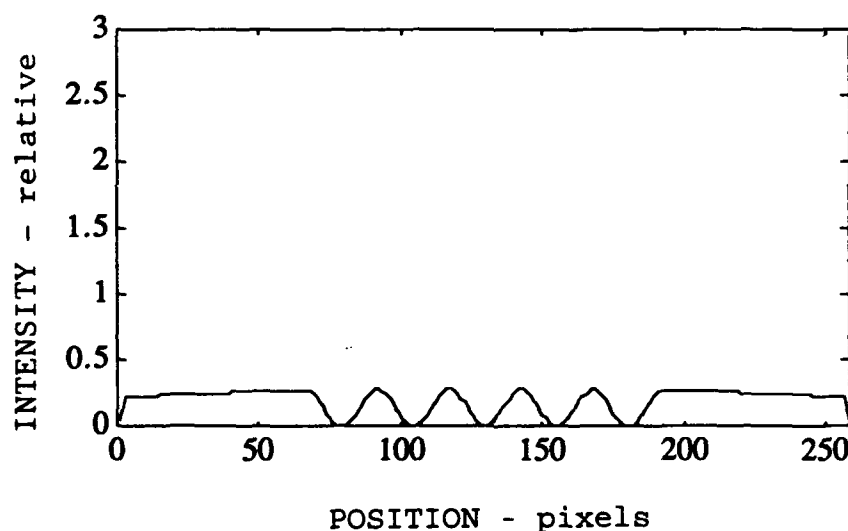
Figure 18. Image Intensity, Field Absorption

c.   Phase Contrast

The phase contrast calculation used Equation 5 with t = 1.
The image is plotted in Figure 19. It is seen that phase
contrast gives an image very similar to dark central ground with
some improvement in both intensity and fringe visibility.   There
is, however, a $\pi/4$ phase shift from the dark central ground
image.   This phase shift is a function of the spot transmittance
and goes to zero when t = 0.   Indeed, dark central ground is a
special case of phase contrast when t = 0. One would have to
account for this phase shift for quantitative data reduction.

22

The phase contrast filter calculation was done for completeness but not used in the experiments described below.

The $\pi/2$ phase shift used for the filter described by Equation 5 was selected because of its use in the phase contrast microscopy. However, for the conditions used here, a phase shift of π gives better results. Figure 20 shows that this filter results in higher intensity fringes, better contrast, no artificial fringe shifts, and a lower background level than any of the previous filters.

Figure 19.   Image of Five Cycle Phase Object using the Phase Contrast Method
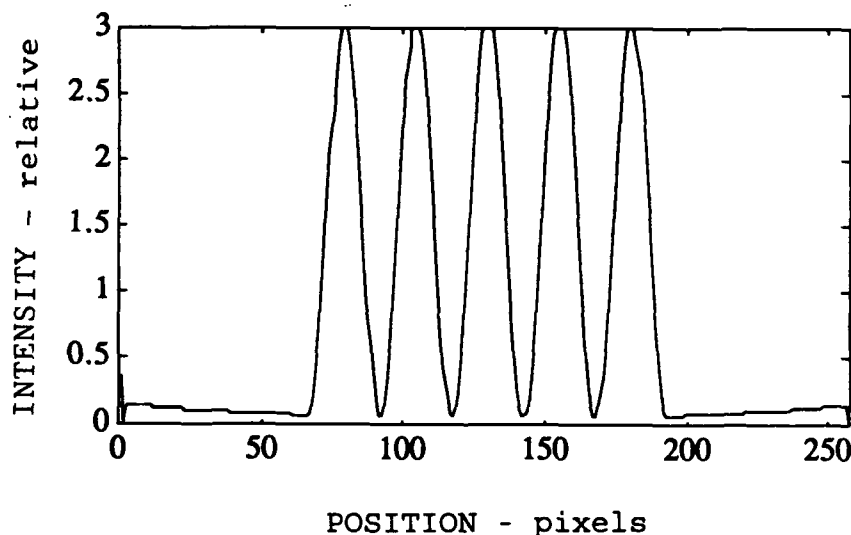
Figure 20.   Phase Contrast Image with a π Phase Shift Filter

23

SECTION IV

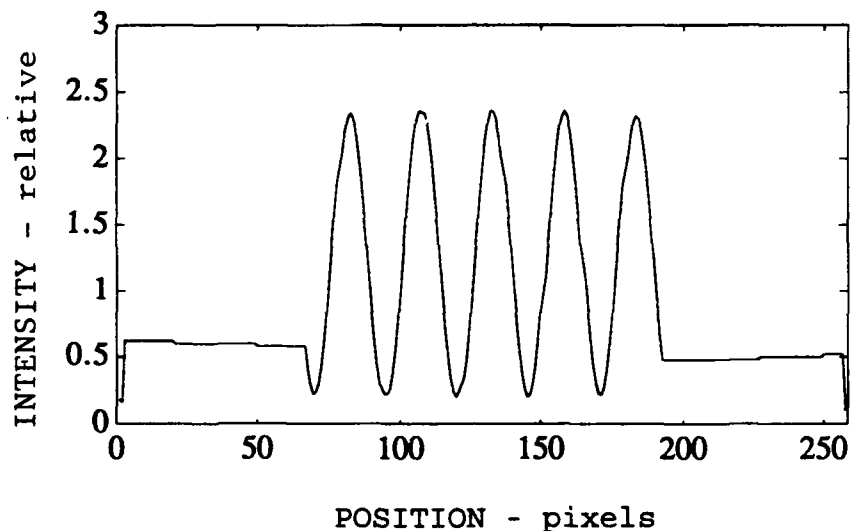## COMMON-PATH INTERFEROMETER STATION

1. EXPERIMENTAL SETUP

Figure 21 is the schematic layout of the optical system used in the ARF. A double pass system was chosen for its increased sensitivity and because it eliminated the astigmatism found in uncorrected 'Z' type layouts. The mirror is 45 cm in diameter with a 610 cm radius of curvature. A Q-switched pulsed ruby laser, which is not of holographic quality, is used as a source. Nominal energy output is 120 millijoules per pulse. L3 is a lens corresponding to L3 in Figure 1.
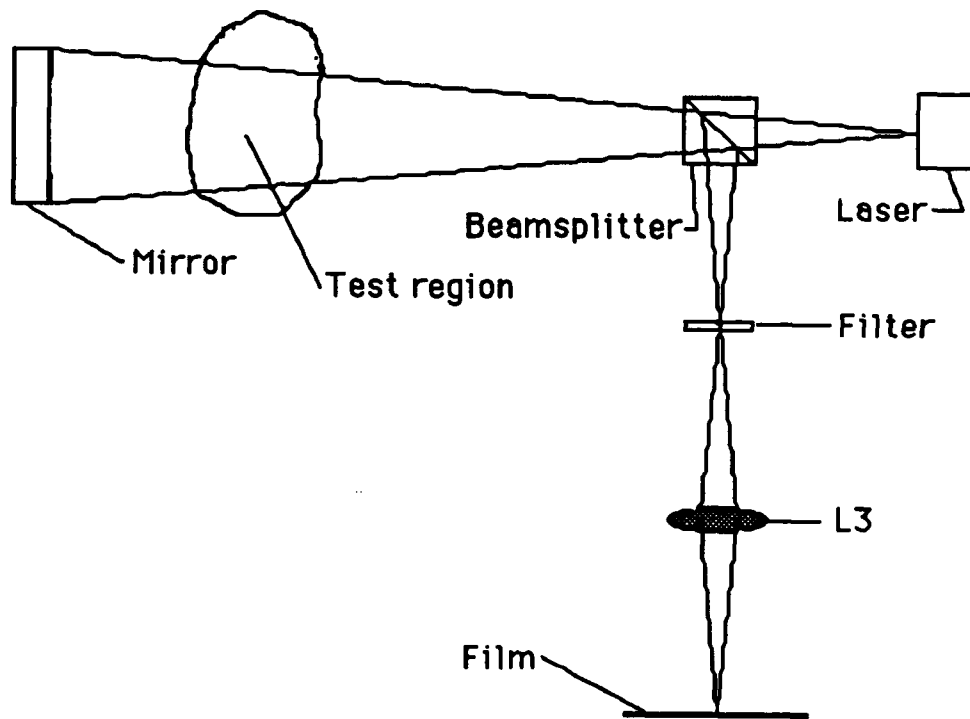
Figure 21. Schematic Layout for the Optical System

Several methods for making the spatial filter have been tried, but a very simple one stands out. The filters are made on holographic plates, which are mounted in the system. To make a dark central ground filter, an unexposed plate is placed with the emulsion at the focus of the primary mirror. This procedure can be performed in room light because development of the plate is not necessary. The laser is flashed with no disturbance in the test region. The high intensity central spike seen in Figure 13 blackens the region it illuminates on the plate. Hence, a

perfectly aligned black dot appears in a fairly transparent field. If a single pulse does not produce a black spot of sufficient size to produce high visibility fringes, additional pulses can be applied until acceptable visibility is achieved.

A field absorption filter can also be made with a photographic plate, but this time the plate is first exposed with uniform light to produce an intensity transmittance near 0.0625 after it is developed. The plate is then mounted with the emulsion at the mirror focus. The central spike now burns a hole through the emulsion, leaving a properly sized, aligned hole surrounded by an absorbing field. The clear hole passing the intense central spike has an advantage in applications where power is so high that any material used to make the dark central dot will burn off the surface on the first shot. However, this advantage is counterbalanced by the fact that the field absorption method has a much lower light efficiency than the dark central ground.

In Section III, the tacit assumption of a diffraction limited system was made. This was not true for the system in Figure 21. However, it has been found that useful interferograms can be obtained even in the presence of some aberrations. In this case, the burned spot was approximately 120 microns--a factor of 5 larger than a diffraction limited spot. The size of a spot is determined by the system blur circle. Motion with respect to this spot will determine the vibration sensitivity. The system has produced interferograms of projectiles launched from 30 calibre, 20-, 40- and 75-millimeter (mm) guns located 30 meters away. Some variability due to vibration has been observed.

SECTION V

EXPERIMENTAL RESULTS

Figures 22 and 23 are interferograms of the flow field around a 20-mm bullet flying at a Mach number of 1.4. Figure 22 was made using a dark central ground spatial filter, while Figure 23 was made with a field absorption filter.
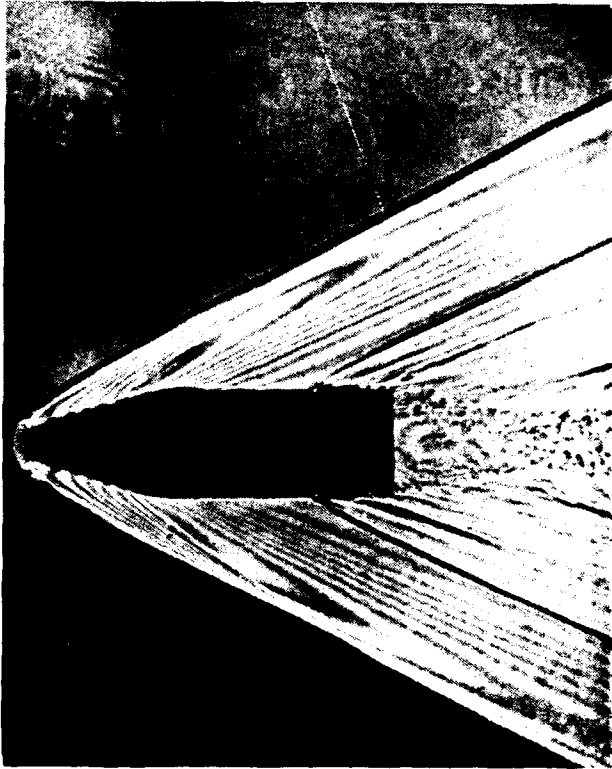

Figure 22. Dark Central
            Ground Interferogram

Figure 23. Field Absorption
            Interferogram

SECTION VI

CONCLUSIONS

Much of the technology required to produce interferograms of projectiles flying in the ARF, without the use of a Mach-Zehnder interferometer, was found to exist in the literature as far back as 1951. The types of interferometers considered fell in two categories: common path and holographic. Each type has its own advantages. Both types are now installed on the ARF and are ready to collect data on a routine basis.

The holographic system used a textbook layout; the problem was to build a system that would work in the hostile environment of the ARF. The major concern was the shock and vibration caused by the guns. It was found that vibrations presented a problem only when the light gas gun was used. The best interferograms were made using this system. A disadvantage was the need to make the hologram in the ARF and then to use it in a separate system to reconstruct the interferogram.

Synthetic interferograms were obtained and are reported herein for comparison with the experimental interferograms. The agreement is excellent and clearly shows the viability of this approach to check CFD calculations for much more complicated flows.

Dark central ground and field absorption common path interferometers that were used required only a single optical system to be installed in the ARF. The type of spatial filter used determined the type of interferometer. A change between the two can be made in a few minutes. In addition, the phase contrast filter was studied. Theoretically, the π phase shifting filter was found to be the best of the common path systems, but so far a good method to make the filter has not been found. It is a new type of filter that has never been used before. This class of interferometers has the advantage of producing the interferograms directly. Therefore can be used to observe real-time events. They are insensitive to vibration and temperature changes. The disadvantage of the common path approach is that the interferograms have not been as sharp as those obtained holographically. While there is no theoretical explanation, the difficulty seems to be in the technology of making the filters.

As an outgrowth of this work, a common path interferometer was installed in the 14 by 14 cm supersonic tunnel at the University of California at Berkeley (Reference 17). This interferometer is in operation and producing useful interferograms. Because the interferograms appear in real time, this wind tunnel installation is useful for studying time-dependent flows. Based upon the Berkeley installation,

researchers at NASA Ames have installed a similar interferometer in one of their tunnels and are collecting time-dependent data.

SECTION VII

RECOMMENDATIONS

Theory indicates that the phase contrast version of these interferometers would be far superior to the other two. Work should continue along this approach. An effort should be made to construct a π phase contrast system to determine if the theoretical predictions are valid.

An effort should be made to generate synthetic interferograms for projectiles at an angle of attack. This method would be helpful to check the CFD codes in a three-dimensional case by use of single view interferograms.

Further consideration should be given to measuring three-dimensional flow by use of tomography. This step will require multiple view interferograms. The problem should be examined, and if feasible, such a system should be designed and constructed.

As an interim step between the single view and the multiple views necessary for tomography, the synthetic interferogram comparison should continue as multiple views become available.

REFERENCES

1.   W.H. Horman, "An Application of Wavefront Reconstruction to Interferometry," Applied Optics, Vol. 4, pp. 333-336, 1985.

2.   R. Prescott and E. L. Gayhart, "Interference Phenomenon in the Schlieren System," Journal Optics Society of America, Vol. 39, pp. 546-550, 1949.

3.   S. R. Erdmann, "A New Simple Interferometer for Obtaining Quantitatively Evaluable Flow Patterns," National Advisory Committee for Aeronautics Technical Memorandum 1363, 1953.

4.   C. M. Vest, Holographic Interferometry, John Wiley & Sons, New York. 1979.

5.   W. Merzkirch, Flow Visualization, Academic Press, New York, Chapter 3, 1974.

6.   B. Butler, D. King, B. Nguyen, and G. Abate, Ballistic Range Flowfield Measurements of the Hypervelocity Near Wake of Generic Shapes and Correlation with CFD Simulations, AIAA 28th Aerospace Sciences Meeting, AIAA paper 90-0621, 1990.

7.   J. W. Goodman, Introduction to Fourier Optics, McGraw-Hill, New York, 1968.

8.   F. Zernike, "Phase Contrast: A Method for the Microscopic Observation of Transparent Objects," Physica, Vol. IX, pp. 686-693, 1942.

9.   R. Bouyer and C. Chartier, "Application of Phase Contrast to the Study of High-speed Gas Jets, "Proceedings of the 3rd International Congress on High-Speed Photography, (R. B. Collins, ed.) Butterworth, England.

10.   M. Philbert, "Visualisation des Ecoulements a Basse Pression," Research Aerospace, Vol 99, pp. 39-48, 1964.

11.   C. Veret, "Vizualisation a Faible Masse Volumique," AGARD Conference Proceedings, No. 38, pp. 257-264, 1970.

12.   R. N. Smartt and John Strong, "Point-Diffraction Interferometer," Journal of the Optical Society of America, 62, p. 737, 1972.

13.   R. N. Smartt and W. H. Steel, "Theory and Application of Point-Diffraction Interferometers," Japan, Journal of Applied Physics, Vol. 14, Supplemental 14-1, 1975.

14. R. C. Anderson and M. W. Taylor, "Phase Contrast Flow Visualization," <u>Applied Optics</u>, Vol. 21, pp. 528-536, 1982.

15. R. C. Anderson and S. Lewis, "Flow Visualization by Dark Ground Interferometry," <u>Applied Optics</u>, Vol. 24, p. 3,687, 1985.

16. R. C. Anderson and J. E. Milton, "A Large Aperture Inexpensive Interferometer for Routine Flow Measurements," <u>International Congress of Instrumentation in Aerospace Simulation Facilities</u>, IEEE Publication 89CH2762-3, pp. 394-399, 1989.

17. M. P. Loomis, M. Holt, G. T. Chapman, and M. Coon, "Application of Dark Central Ground Interferometry," AIAA 29th Aerospace Sciences Meeting, AIAA paper 91-0565, 1991.

DISTRIBUTION LIST
(WL-TR-92-7035)

Defense Technical Info. Center
DTIC/DDAC
Cameron Station
Alexandria VA 22304-6145
2

Eglin AFB offices:

WL/CA-N   1
WL/MNOI (Scientific and Tech.   1
                     Info. Facility)

AUL/LSE
600 Chennault Circle, Bldg. 1405
Maxwell AFB AL 36112-5564
1

WL/FIES/SURVIAC
Wright-Patterson AFB OH
45433-7562
1

AFSAA/SAI
1580 Air Force Pentagon
Washington DC 20330-1580
1

ASC/ENSTA
Wright-Patterson AFB OH
45433-6553
1

Det 1, 7454 TIS/INTSW
APO NY 09094-5001
1

ASC/XRH
Wright-Patterson AFB OH
45433 6503
1

NASA Ames Research Center
Attn: Dr. Tony Strawa, MS 229-3
Moffett Field CA 94035-1000
1

Wright-Patterson AFB OH
45433-6523
1

Eglin AFB offices:

WL/CA-F	1
WL/FIM	1
WL/FIB	1
WL/FIGX	1
WLFIGCC	1
WL/TXA	1

WL/MNAA	4
WL/MNAG	1
WL/MNAV	1
WL/MNM	1
WL/MNPX	1
WL/MNSI	1
ASC/XREWD	1

NASA Langley Research Center
Technical Library Branch, MS 185
Attn: Document Cataloging
Hampton VA 23665
1

HQ AFIA/INT
Bolling AFB DC 20332-5000
1

EOARD/LDV
Box 14
FPO NY 09510-0200
1

Commander
U.S. Army Missile Command
Redstone Science Information Center
Attn: AMSMI-RE-CS/R Documents
Redstone Arsenal AL 35898-5241
1

Commander
Naval Weapons Center (Code 3431)
Attn: Technical Library
China Lake CA 93555-6001
1